Supplementary Information for "Optical and spin coherence of Er spin qubits in epitaxial cerium dioxide on silicon"

Jiefei Zhang,[1,2,*] Gregory D. Grant,[3,1] Ignas Masiulionis,[3,1] Michael T. Solomon,[3,1,2] Jonathan C. Marcks,[1,2,3] Jasleen K. Bindra,[4] Jens Niklas,[4] Alan M. Dibos,[5,6,2] Oleg G. Poluektov,[4] F. Joseph Heremans,[1,2,3] Supratik Guha,[3,1,2,†] and David D. Awschalom[3,1,2,7]

[1] *Materials Science Division, Argonne National Laboratory, Lemont, Illinois 60439, USA*
[2] *Center for Molecular Engineering, Argonne National Laboratory, Lemont, IL 60439, USA*
[3] *Pritzker School of Molecular Engineering, University of Chicago, Chicago, Illinois 60637, USA*
[4] *Chemical Sciences and Engineering Division, Argonne National Laboratory, Lemont, IL 60439, USA*
[5] *Nanoscience and Technology Division, Argonne National Laboratory, Lemont, Illinois 60439, USA*
[6] *Center for Nanoscale Materials, Argonne National Laboratory, Lemont, Illinois 60439, USA*
[7] *Department of Physics, University of Chicago, Chicago, Illinois 60637, USA*

(Dated: Friday 13th September, 2024)

S1. Confocal optical setup

The optical data shown in Fig. 1 and Fig. 2 are measured using a confocal microscopy setup schematically shown in Fig. S1. The sample is mounted in a close-cycle cryostat (Montana Instrument, s50) with a base temperature $\sim$ 3.3 K and a sample temperature $\sim$ 3.6 K. A continuously tunable C-band laser with a 1460 nm –1570 nm tuning range (Toptica CTL 1500) is used for optical excitation. The laser is coupled to a single-mode fiber and sent through multiple optical modulators to create optical excitation pulses of various length and frequency modulation depending on the requirements of various types of optical measurements. For photoluminescence excitation (PLE) measurements, the laser light is modulated by two fiber-based acousto-optic modulators (AOM, AA opto-electronic) with a rise time of about 30 ns and extinction > 45 dB to generate clean 1.5 ms excitation pulse. For photon echo measurements, a fiber-based intensity electro-optic modulator (EOM, iXblue) with a rise time <1 ns and extinction of 36 dB is used to generate 10 ns ($\pi/2$) and 20 ns (π) pulses. The two acousto-optic modulators are also used to envelope the $\pi/2 - \tau - \pi$ time window in order to further cut down on laser leakage to further increase the needed signal-to-noise. The setup can achieve a shortest τ of around 150 ns, without compromising on the extinction level and subsequent signal-to-noise.

The modulated laser is sent through a 50/50 beamsplitter and then focused on the sample using an infrared objective with NA 0.65. Photoluminescence (PL) from the sample is collected by the same objective, passed through the 50/50 beamsplitter, filtered by two 1500 nm long pass filters, and then coupled into a single mode fiber connected to superconducting nanowire single-photon detector (SNSPD, Quantum Opus) for detection. A fiber-based acousto-optic modulator (AOM, AA opto-electronic) with a rise time of about 30 ns is attached to a single-mode fiber to time-gate the photon detection. The AOM on the collection side, as well as the AOM and EOM on the excitation side is controlled by the data acquisition system (DAQ, National Instruments) to set up the properly aligned sequence of collection window with respect to excitation sequences. A collection window of 7 ms opening right after the end of the 1.5 ms optical excitation pulse is used to time-gate and collect the PL from Er ions for PLE measurements. Similarly, a collection window of 860 ns after the end of the 24 ns π-pulse is used for photon echo measurements.

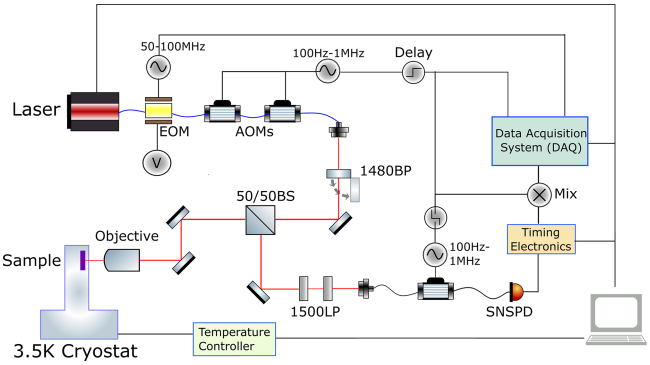

Fig. S1. Schematic of the home-build confocal optical setup used for PLE and photon echo measurements in this work.

S2. Crystal field split energy levels of Er ions

Our prior work [1] indicates that the crystal field in CeO_2 has a cubic symmetry, as expected. Therefore, the 4f-4f transitions in the Er^{3+} ion's first two spin-orbit split multiplets, $^4I_{15/2}$ and $^4I_{13/2}$, are split into 5 levels [1, 2], labeled as Z_1 to Z_5 and Y_1 to Y_5 in the order from the lowest to the highest energy, as schematically shown in Fig. S2(a) (same as shown in Fig. 1(a), recaptured here for completeness).

The crystal field split levels Z_1 to Z_5 and Y_1 to Y_5 are

* jfzhang@anl.gov
† sguha@anl.gov

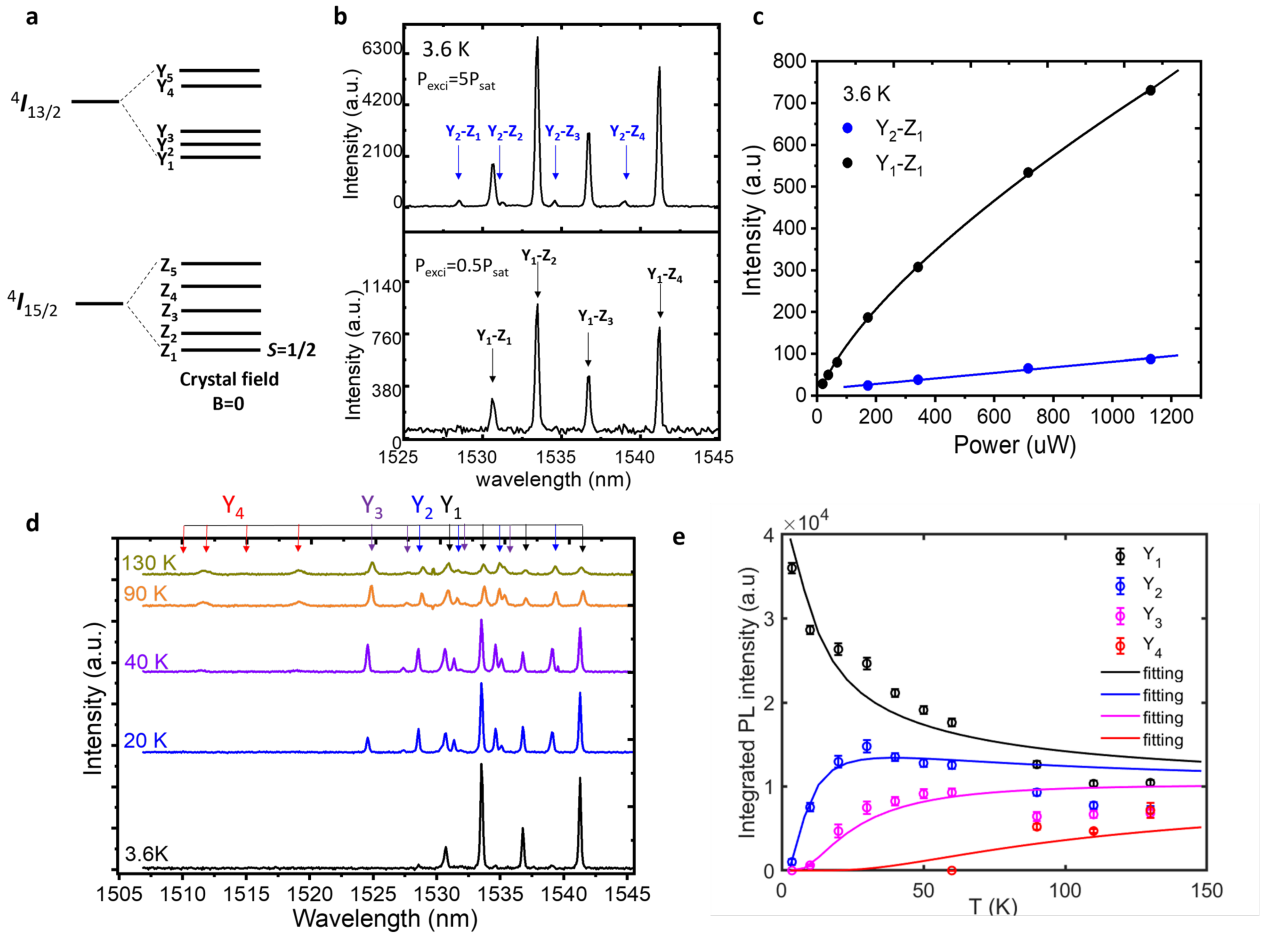

Fig. S2. Crystal field split states of Er^{3+} $^4I_{15/2}$ and $^4I_{13/2}$ multiplets. (a) schematic of the energy diagram of the $^4I_{13/2} \rightarrow^4 I_{15/2}$ transition. (b) PL spectrum of Er emission with Er excited at two different excitation power ($P = 0.5P_{\rm sat}$ and $P = 5P_{\rm sat}$, $P_{\rm sat} \sim 200\mu$W on sample) at 3.6 K. (c) PL intensity of $Y_1 - Z_1$ and $Y_2 - Z_1$ transition as a function of excitation power at 3.6 K. (d) Temperature dependent PL spectrum obtained at excitation power, $P = 5P_{\rm sat}$. (e) Integrated intensity of PL emission from Y_1, Y_2,Y_3 and Y_4 to all Z levels (Data are shown as open circles with fittings using Eq. 1 shown as solid lines.

probed and identified through temperature and power dependent PL measurements with 20 GHz (0.16 nm, 84 μeV). Er^{3+} ions are excited by CW laser excitation at 1473 nm with energy higher than $^4I_{13/2} \rightarrow^4 I_{15/2}$ transition. At 3.6 K, PL occurs primarily from Y_1 to all the Z levels due to the rapid non-radiative relaxation of electrons from higher Y levels to Y_1 level. Four emission peaks are observed in Fig. S2(b) (marked with black arrows). These are identified to be Y_1 to $Z_1 - Z_4$ transitions. With increasing excitation power, increasing population of electrons to higher Y level, Y_2, are created leading to PL from Y_2 to $Z_1 - Z_4$ level transitions (four more peaks marked by blue arrows). The confirmation of these being from Y_2 levels comes from the fixed energy separation of the observed Y_2 and Y_1 to Z level transitions and the power dependence of PL intensity of $Y_1 - Z_1$ and $Y_2 - Z_1$ transition, as an example, shown in Fig. S2(c).

The identification of Y_2 level is also confirmed with temperature dependent PL behavior. Fig. S2(d) shows the PL spectrum measured at temperatures ranging from 3.6 K to 130 K. It is the same as Fig. 1(b) and is reproduced here for continuation of discussion. At temperatures above 15 K, the same four Y_2 to Z_1 to Z_4 level transition peaks (marked by blue arrows in Fig. S2(b) and (d)) show up with their intensity increasing with temperature, while the PL intensities from Y_1 to Z_1 to Z_4 level transitions (black arrows in Fig. S2(b) and (d)) decrease with increasing temperature (Fig. S2(d)). With continued increase of temperature, higher Y levels get populated. Four additional set of peaks (marked by purple arrows in Fig. S2(d)) emerge when temperature is above 40 K. These four peaks are assigned as Y_3 to Z_1 to Z_4. With temperature above 50 K, higher Y_4 transitions are also observed. The table shown in in Fig. 1 in main text captures the summery of deduced crystal field split Y and Z levels of the $^4I_{13/2}$ to $^4I_{15/2}$ transitions.

The intensity of Y_1 to Y_5 transitions as a function of temperature is consistent with Boltzmann distribution

of electrons. Fig. S2(e) shows the PL emission intensity from all four Y levels as a function of temperature. The lines are the fit to the data using the following equation:

$$I_{Y_j} \propto \frac{exp(-(E_{Y_j} - E_{Y_1})/K_B T)}{\sum_{j=1}^{j=5} exp(-(E_{Y_j} - E_{Y_1})/K_B T)} \quad (1)$$

where E_{Y_j} is the energy of j-th Y level, k_B is the Boltzmann constant, T is temperature. The fit is done using the energy separation between the Y levels deduced from PL measurements as input constants to Eq. 1. We find that the fit is consistent with the observed temperature dependent PL signal from the involved transitions, confirming the assignment of crystal level split states.

S3. Photon echo measurements

To reduce dephasing induced through excitation pulse, we use 20 ns π pulse and 10 ns $\pi/2$ pulse, the shortest clean pulses from the setup. The laser is resonant on the $Y_1 - Z_1$ transition with a bandwidth of 5 MHz, controlled by the pulse length. The identification of pulse area to π is achieved by tuning the laser power while measuring the overall integrated echo intensity with a fixed $\tau = 150$ ns. Fig. S3 shows the measured integrated echo intensity as a function of laser power incident on the sample. The integrated echo amplitude increases with excitation power till it reaches π pulse. The measured data indicate that the π pulse area is reached with excitation power close to the maximum achievable power of 425 μW from our setup. All two-pulse photon echo measurements reported in Fig. 2 are done with power of 425 μW on the sample.

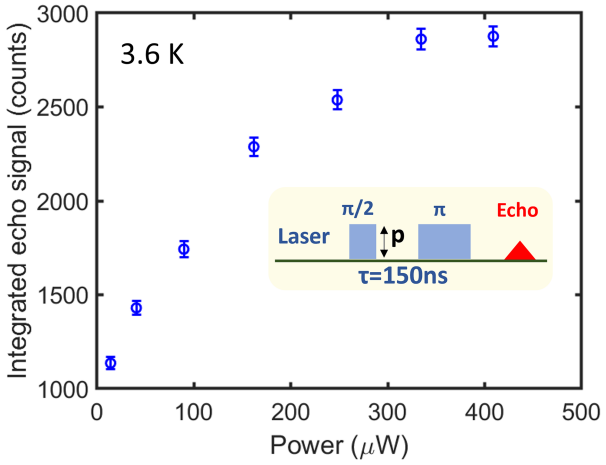

Fig. S3. Integrated photon echo amplitude as a function of excitation power (p) on sample indicating π pulse area reached with power around 420 μW

S4. Pulsed EPR instrumentation

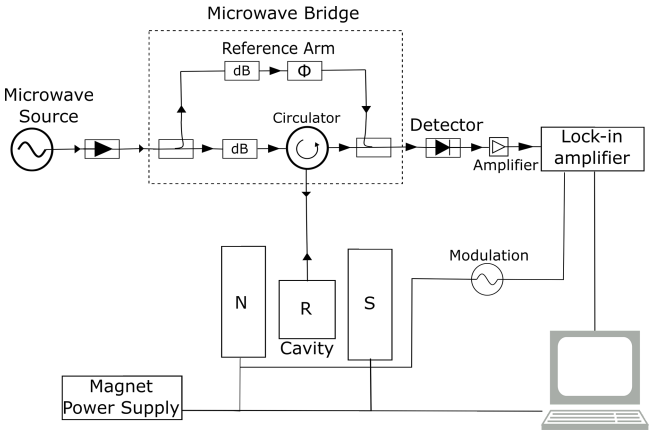

Fig. S4. Schematic of the pulsed EPR setup used for the study of Er spin coherence and relaxation reported in the main text.

Pulsed EPR measurements are carried out using Bruker's ELEXSYS E580 spectrometer. The schematic of the setup is shown in Fig. S4. The sample is diced into a 25mm x 1.5mm strip and loaded into an EPR tube. The tube is inserted in and coupled to the dielectric ring resonator (Bruker ER 4118X-MD5). The microwave pulses are generated from the microwave bridge and applied to the resonator. The cavity mode with uniform RF magnetic field along the sample's longitudinal axis is used as pumping mode driving the RF absorption in the sample [3]. The corresponding magnetization of the electron spins is measured in the form of an emitted microwave signal, which is amplified by the cavity before detection. The change of magnetization of spins as a function of time with different pulse sequences are measured for the study of Er spin coherence and relaxation dynamics reported in the main text.

S5. Instantaneous diffusion measurements

In instantaneous diffusion measurements, generalized Hahn echo sequences ($\pi/2 - \tau - \theta$, schematic shown in Fig. 3(c)) are performed with the fidelity of the second inversion pulse (θ) varied [4] to identify the effect of Er spin dipolar interaction on ensemble decoherence. To ensure the probed spin ensemble size being constant, we have kept the second rotation pulse length as a constant 12 ns with the rotation angle (θ) adjusted by reducing the microwave (MW) power. The pulse width for the $\pi/2$ pulse is thus increased such that the pulse area remains $\pi/2$. We first identify the pulse area by applying standard Hahn-echo sequence while maximizing the spin echo signal at fixed τ of 100 ns through fine tuning of microwave power. Then we switches to instantaneous diffusion measurement by reducing the second rotation pulse length down to 12 ns. Table. I below shows the

three measurement conditions for data in Fig. 3(c).

MW attenuation (dB)	$\pi/2$ pulse (ns)	θ pulse (ns)	θ
-19	12	12	90°
-24	24	12	50.6°
-28	36	12	31.9°

TABLE I. Measurement condition and extracted rotation angle θ of instantaneous diffusion measurements.

The rotation angle shown in the table is calculated by computing the ratio of pulse area of the second rotation pulse to the $\pi/2$ pulse using the following Eq. 2:

$$\theta = \pi/2 * 10^{(P_{\pi/2} - P_{\text{att}})/20} \tag{2}$$

where $P_{\pi/2}$ is the MW attenuation for θ angle of 90° and P_{att} is the MW attenuation for the other rotation angles.

For each rotation angle, general Hahn-echo sequence ($\pi/2 - \tau - \theta$) is applied with τ ranging from 100 ns to 1300 ns where 100 ns is the limit of the smallest τ achievable in the pulsed EPR spectrometer. The echo signal is proportional to the exponential of the averaged inversion pulse fidelity $< \sin^2(\theta/2) >$ with the spin $T_{2,\text{INST}}$ linearly proportional to $< \sin^2(\theta/2) >$ as shown in main text with the following relationship:

$$SE(\tau) \propto exp(\frac{8\pi^2}{9\sqrt{(3)}} \frac{g^2\beta^2}{\hbar} N \sin^2(\theta/2)\tau) \tag{3}$$

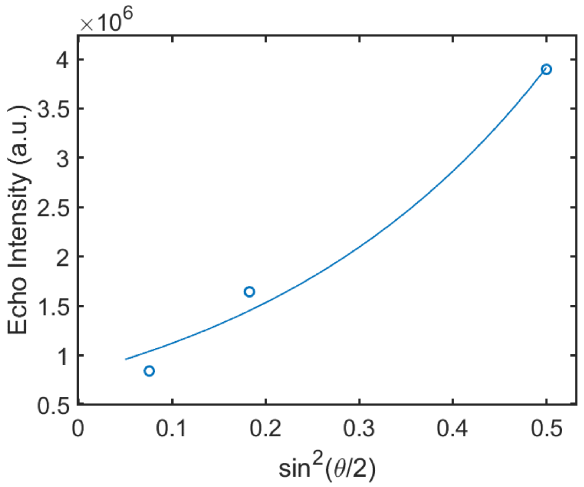

Fig. S5. Spin echo signal at $\tau = 100$ ns the three different averaged inversion pulse fidelity $< \sin^2(\theta/2) >$. The solid line is a fit to the data using Eq. 3.

Fig. S5 shows the plot of the echo signal at $\tau = 100$ ns as a function of the average inversion pulse fidelity $< \sin^2(\theta/2) >$. The solid line is a fit to the data using Eq. 3. The extracted N sampled by the generalized echo sequence is $2.08 * 10^{22}/m^3$. Considering the pulse only probes $\sim$ 12% of the spins within the inhomogeneous distribution, the estimated total concentration of the Er spin is $\sim$ 6 ppm, consistent with the value extracted from T_2 data shown in Fig. 3(d).

S6. Possible processes limiting $T_{2,bath}$

Based on the instantaneous diffusion measurements, the dephasing due to Er ion-ion interaction governed by $T_{2,INST}$ is found to be $\sim$ 0.426 μs with $T_{2,bath}$ being around 0.66 μs at 3.6 K. The Er ion-ion interaction is clearly one of the dominating factor for dephasing. With further reduction of Er concentration down to single ion limit, one could have $T_2 = T_{2,bath} = 0.66$ μs at 3.6 K. Now we try to access contributing factor for $T_{2,bath}$. As noted in the main text, the $T_{2,bath}$ represents the combined effect of dephasing due to coupling to phonon, magnetic TLS and interaction of Er with possible magnetic defects as represented in Eq. 4 below:

$$1/T_{2,bath} = 1/T_1 + 1/T_{TLS} + 1/T_{ion-spin} \tag{4}$$

The observed millisecond spin T_1 indicates that the dominating limiting factor for $T_{2,bath}$ is from coupling to magnetic TLS and interaction of Er with other spin defects. From the temperature dependent study of optical coherence, the coupling to TLS should lead to $T_{TLS} > 10$ μs ($<$ 15 kHz). Thus, the dominating processes limiting $T_{2,bath}$ is coupling of Er to spin defects in the grown CeO_2 film.

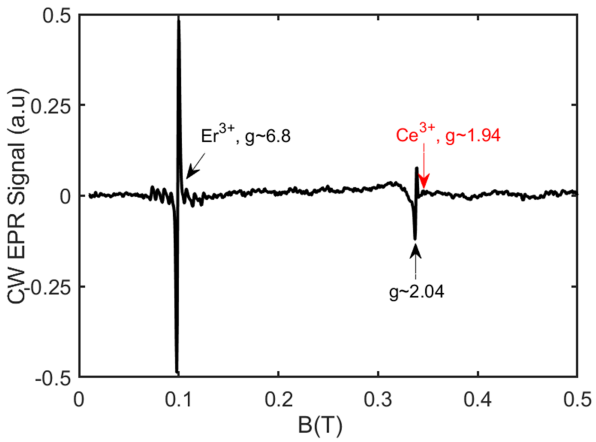

Fig. S6. CW EPR spectrum of the studied Er doped CeO_2 at 3.6 K

Broad band CW EPR data is obtained from the 3 ppm Er doped CeO_2 sample at 3.6 K to probe on possible spin defects in the sample. Fig. S6 shows the measured result obtained with B field parallel to sample (111) surface. The lack of spin resonance with g-factor around 1.94(6) (marked by a red arrow) indicates that there is no detectable signal from Ce^{3+} [5, 6]. It suggests that the concentration of Ce^{3+} in the sample is much lower compared to Er concentration and is below the detection limit of EPR. The resonance observed with g around 2.04 could be coming from oxygen vacancies and defect clusters [7, 8]. Further careful examination of this resonance as a function of Er concentration and annealing temperature is needed to find the origin of the observed spin

resonance. The results indicate presence of as-grown defects that could interact with Er ion causing dephasing.

All these suggests that one could reduce $T_{ion-spin}$ with growth optimization and post-growth treatment in reducing unintended defects and enhance spin $T_{2,bath}$ to above 10 μs at 3.6 K, limited by possible coupling to TLS. It also indicates that one can further improve on $T_{2,bath}$ by reducing temperature to sub-kelvin to freeze out coupling to magnetic TLS and reach T_1 limited coherence of millisecond time scale.

S7. Optical measurements of spin relaxation

The optical measurements probing spin relaxation dynamics are carried out in a dilution refrigerator using a 3-axis 250 mT–250 mT–250 mT vector magnet with fiber-coupled optical access as shown in Fig. S7. For direct comparison with pulsed EPR data in Fig. 4(a), we carry out all measurements at 3.6 K with a magnetic field along the same crystal direction of $\langle 1-10 \rangle$. The sample is mounted on the MXC flange inside the dilution refrigerator. A single mode fiber is used for optical excitation and collection. A fiber circulator is used in the optical path to separate excitation pulses from fluorescence. Excitation laser and collected fluorescence are routed to our confocal setup shown in Fig. S1 for measurements.

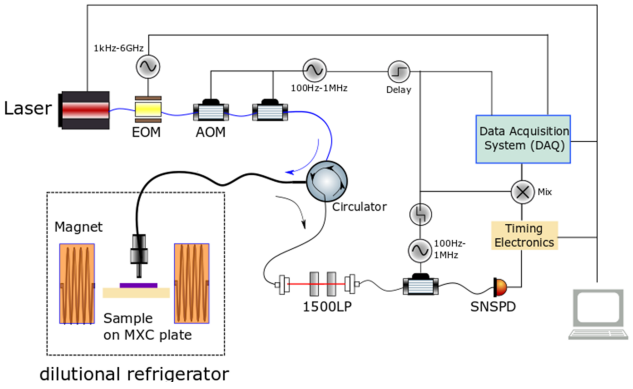

Fig. S7. Schematic of the optical setup with the dilution refrigerator for optical measurement of spin relaxation dynamics.

A 100 μs pulse at wavelength resonant to the Z_1 spin-down level to the Y_1 spin-up level is applied first. The excitation wavelength is estimated based on the g factor of the Er ions. The first pulse excites electrons occupying the Z_1 spin-down level to excited states to create more population of electrons at Z_1 spin-down level at 3.6 K after the pulse. The pulse length is chosen to be longer than optical π pulse for improved optical contrast but also short enough that emission from $Y_1 - Z_1$ transition does not alter electron distribution between the Z_1 spin-up and spin-down states. The relaxation of spin-up to spin-down is picked out by the second 100 μs pulse after time τ through exciting the electrons at spin-down level and tracking the subsequent emission, sequence shown in Fig. S8(a). Given the spin T_1 is shorter than the optical lifetime of the $Y_1 - Z_1$ transition, one should sample and subtract the emission collected in the collection window due to the radiative decay process after the first optical pulse. Therefore, a reference measurement with only the first pulse is carried out for background subtraction. The population recovery of spin-up to spin-down state is probed through the measurement of the difference in counts (ΔPL) as a function of time delay τ. Using the pulse sequence shown in Fig. S8(a), ΔPL as a function of time delay τ is measured with magnetic field strength at 100 mT (Fig. 4(b)).

To probe the effect direct spin-lattice coupling has on spin relaxation, we carry out measurements of spin relaxation T_1 at various magnetic field strengths (i.e. 50 mT, 100 mT, 150 mT, and 250 mT). Fig. S8 shows the measured $\Delta PL(\tau)$ at different magnetic field strength. Spin T_1 is extracted through a single exponential fit (solid line) with 95% confidence fit.

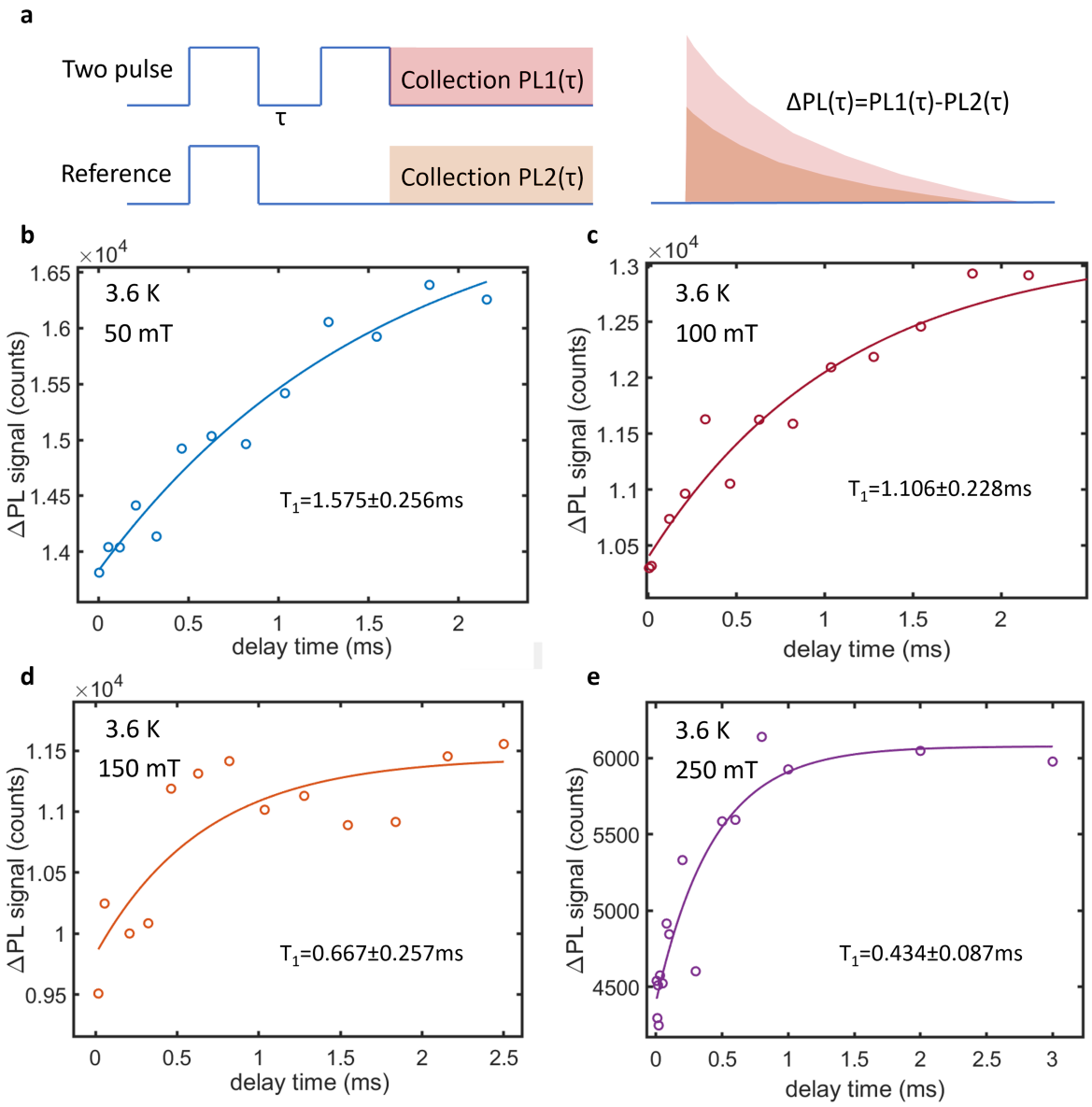

Fig. S8. Optically probed spin T_1. (a) Two pulse sequences used for optically proved spin T_1. The optical pulse is of 100 μs with delay time, τ, between the two pulses. The collection window of 4 ms opens after the second optical pulse. The collected signal difference between the two-pulse measurement and reference measurement (ΔPL) represents the population recovery of Z_1 level spin-down level due to relaxation. Panel (b)-(d) shows the ΔPL measured as a function of time delay τ at a magnetic field strength of (b) 50 mT—yielding a spin $T_1 = 1.575 \pm 0.256$ ms. (c) 100 mT—yielding a spin $T_1 = 1.106 \pm 0.256$ ms (same as the one shown in Fig. 4(c)). (d) 150 mT—yielding a spin $T_1 = 0.667 \pm 0.257$ ms and (e) 250 mT—yielding a spin $T_1 = 0.434 \pm 0.087$ ms.

[1] G. D. Grant, J. Zhang, I. Masiulionis, S. Chattaraj, K. E. Sautter, S. E. Sullivan, R. Chebrolu, Y. Liu, J. B. Martins, J. Niklas, A. M. Dibos, S. Kewalramani, J. W. Freeland, J. Wen, O. G. Poluektov, F. J. Heremans, D. D. Awschalom, and S. Guha, Optical and microstructural characterization of Er3+ doped epitaxial cerium oxide on silicon, APL Materials **12**, 021121 (2024).

[2] C. A. J. Ammerlaan and I. de Maat-Gersdorf, Zeeman splitting factor of the Er3+ ion in a crystal field, Appl. Magn. Reson. **21**, 13 (2001).

[3] M. Huisjen and J. S. Hyde, A pulsed EPR spectrometer, Review of Scientific Instruments **45**, 669 (1974).

[4] K. Salikhov, S. Dzuba, and A. Raitsimring, The theory of electron spin-echo signal decay resulting from dipole-dipole interactions between paramagnetic centers in solids, J. Magn. Reson. **42**, 255 (1981).

[5] R. Rakhmatullin, V. Semashko, S. Korableva, A. Kiiamov, A. Rodionov, R. Tschaggelar, J. van Bokhoven, and C. Paun, Epr study of ceria nanoparticles containing different concentration of ce3+ ions, Materials Chemistry and Physics **219**, 251 (2018).

[6] E. Abi-Aad, A. Bennani, J.-P. Bonnelle, and A. Aboukaïs, Transition-metal ion dimers formed in ceo2: an epr study, J. Chem. Soc., Faraday Trans. **91**, 99 (1995).

[7] J. Soria, A. Martínez-Arias, and J. C. Conesa, Spectroscopic study of oxygen adsorption as a method to study surface defects on ceo2, J. Chem. Soc., Faraday Trans. **91**, 1669 (1995).

[8] D. Woodruff, ed., *Oxide Surfaces*, The Chemical Physics of Solid Surfaces, Vol. 9 (Elsevier, 2001) p. ii.